Bistable/Oscillatory System Based on the Electroreduction of Thiocyanate Complexes of Nickel(II) at a Streaming Mercury Electrode. Experiment and Simulation

Rafał Jurczakowski and Marek Orlik*

Laboratory of Electroanalytical Chemistry, Department of Chemistry, University of Warsaw, ul. Pasteura 1, PL-02-093 Warsaw, Poland

Received: September 10, 2001

Oscillatory electroreduction of the thiocyanate complexes of nickel(II) at stationary mercury electrodes is complicated by the formation and accumulation of the heterogeneous Ni amalgam and a surface active NiS adsorbate. Consequently, dynamic instabilities observed at such electrodes always have a transient character. To overcome these difficulties, following our previous studies of the Ni(II)-SCN^- oscillator, we describe the new experimental approach, based on the application of the *streaming* mercury electrode to the studies of nonlinear dynamic instabilities of this system. A special experimental setup was assembled. We found that in the presence of an appropriate serial ohmic resistance in the electric circuit, not only the sustained oscillations, but also the *bistable* behavior in the current−voltage characteristics occurred, which was not reported for this process so far. The experimental diagram of regions of the bistability, monostability and oscillations in the $U-R_s$ parameter space is constructed. For the explanation of the bistability, the numerical models were elaborated which quantitatively confirmed the observed phenomena as originating from the coupling of the negative differential polarization resistance with ohmic potential drops.

1. Introduction

Studies of various nonlinear dynamical systems, in which self-organization (formation of dissipative structures) occurs, are of great importance for the explanation of many natural processes and for the modern understanding of the concept of irreversibility.[1,2] Real chemical systems are as a rule nonlinear, so a large number of chemical processes is expected to exhibit various kinds of self-organization in appropriate conditions.

In particular, electrochemical oscillators[3−5] constitute an important class of nonlinear dynamical systems, for which the deviation from the thermodynamic equilibrium can be easily and smoothly realized by the change of the applied electrode potential or the imposed current density. Numerous examples of self-organization in electrochemical systems were reported for the voltammetric, chronoamperometric, or chronopotentiometric studies of various electrode processes, usually exhibiting an explicit or hidden negative faradaic impedance in their current−voltage ($I-U$) characteristics.[3−6] Such processes may also lead to the formation of spatiotemporal patterns.[6] In a specific case, the thin-layer electrolysis of the solution of a low electric conductivity can induce luminescent convective structures of the electrohydrodynamic origin,[7−11] resembling the classical phenomena known as the Bénard−Rayleigh instabilities in thermal convection.[12,13]

Both nonelectrochemical and electrochemical systems exhibit common types of nonlinear dynamic instabilities. An example of such a behavior that can be found in completely different systems, is *bistability* (or, more generally, multistability) which, according to earlier numerous studies, is in many cases strongly related to oscillations (cf. e.g., the Boissonade−de Kepper model[14]).

Our new experimental realization and theoretical analysis of the electrochemical bistable/oscillatory system is described in this paper. It is based on the electroreduction of thiocyanate complexes of nickel(II) at mercury electrodes, which process involves two parallel reaction pathways:[15−18] formation of the nickel(0) amalgam (from the Ni^{2+} electroreduction) and the surface accumulation of the solid NiS layer (from the reduction of SCN^- ligands). One should emphasize that in our previous papers[19,20] we analyzed *transient* oscillations in the Ni(II)-SCN^- electroreduction because only such ones could be observed at the stationary mercury drop electrode. Although, theoretically, at such a spherical electrode the nonzero steady-state current (or sustained oscillations) should be asymptotically attained due to the characteristics of the spherical diffusion, the accumulation of the nickel(II) sulfide, forming a compact, growing inhibitory layer on the mercury surface, constantly depresses the current. It appears that it is difficult to find in practice such experimental conditions for which the side effects of NiS at a stationary electrode could be neglected. Also, the constant accumulation of the heterogeneous nickel(0) amalgam inside the relatively small mercury drop does not allow to continue the experiment for the times long enough to attain and to study the true steady-state or more complex behaviors. To overcome these difficulties, having been forced to keep mercury as the electrode material (due to relatively negative electroreduction potentials of Ni(II)-SCN^-), we replaced the stationary electrode by its nonstationary equivalent: the *streaming mercury electrode*, for which the steady-state mixed convective-diffusion transport ensures both permanent supply of the reactant to the electrode and removal of the undesirable reaction products.

In this paper, we describe representative results of our experiments with a streaming electrode and of numerical calculations, which quantitatively explain the mechanism of the observed bistable phenomena.

2. Experimental Section

The solutions of nickel(II) thiocyanate complexes were prepared *ex tempore* by mixing of appropriate amounts of

* To whom correspondence should be addressed. E-mail: morlik@chem.uw.edu.pl. Fax: +48 22 822 59 96. Phone + 48 22 822 02 11 ext. 245.

10.1021/jp013452m CCC: $22.00
Published on Web 01/15/2002

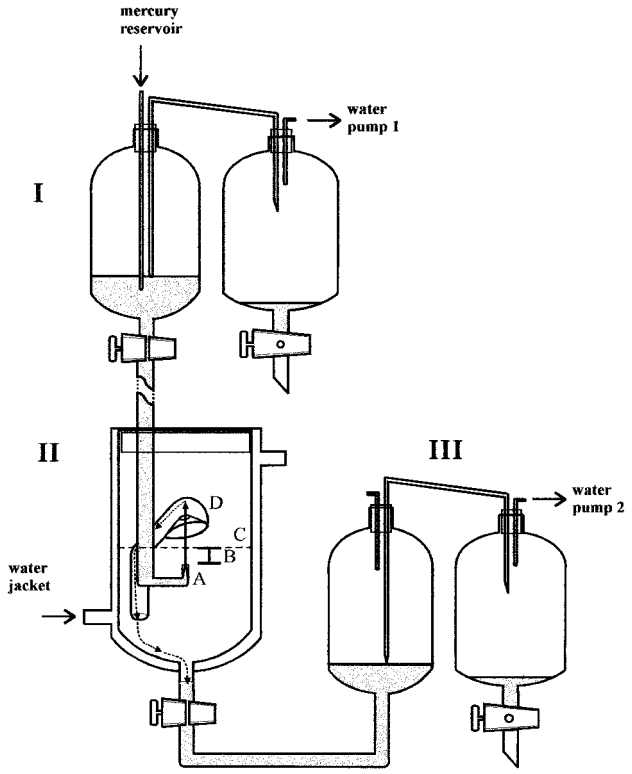

Figure 1. Schematic construction of the experimental setup with the streaming mercury electrode for studying of the dynamic instabilities in the electroreduction of the Ni(II)-SCN^- complexes. **I** − system of maintaining the constant mercury pressure in the flowing stream, **II** − the electrolytic cell, **III** − system of mercury collection, maintaining the constant level of the solution in the electrolytic cell; **A** − glass capillary tip, at which the thin mercury jet is formed, **B** − the proper streaming electrode, i.e., the range of mercury jet of a length l_{max} being in contact with studied solution, **C** − solution surface. The stream of the used mercury is further captured by the fixed element **D** and directed to the bottom part of the cell (see text for additional description).

aqueous solutions of nickel(II) perchlorate with the solution of sodium thiocyanate. Crystalline nickel(II) perchlorate, $Ni(ClO_4)_2 \times 6H_2O$ was obtained by neutralization of the p.a. basic nickel-(II) carbonate (POCh, Poland) with the appropriate amount of p.a. perchloric acid (APOLDA), followed by recrystallization from triply distilled water. The concentration of Ni^{2+} in the stock solution of this salt was determined by complexometric titration with EDTA.[21] Commercially available p.a. NaSCN (Fluka) was purified by recrystallization from water and the concentration of the stock solution was determined by measurements of its density and comparison with literature data.[22] All solutions were prepared with triply distilled water, purified in a final step using Millipore filters.

For the streaming Hg electrode, the commercially available p.a. mercury (POCh, Poland) was used. The schematic construction of the experimental setup with the streaming mercury electrode, assembled by us, is sketched in Figure 1. One should emphasize that a particular effort has been put into making this arrangement suitable for the studies of intrinsic dynamic instabilities of the electrode processes. This means that the construction of the electrode should guarantee that its hydrodynamic characteristics will remain constant as a function of time, even for long-lasting experiments. The streaming electrode should thus be formed by a mercury under a constant pressure, and also the level of the solution in the electrolytic cell should remain unchanged. This was realized by introducing of the construction elements I and III, respectively, shown in Figure 1. The proper streaming electrode appears at the capillary outlet (**A**) and has a form of the thin ($\phi = 0.11$ mm) mercury jet which remains in contact with the studied solution at the distance l_{max} denoted as **B** in Figure 1. The jet then jumps over the surface of the solution (**C**) and is eventually captured by the specially modeled tube (**D**), collecting and directing the used portion of a liquid metal to a bottom of the solution. Thanks to this element **D** the dispersed, falling mercury drops do not induce the side convection (perturbation) of the solution in the close vicinity of the working part of the streaming electrode, what could produce undesirable, stochastic instabilities in the behavior of the studied process.

Using this streaming electrode, chronoamperometric *I-t* and voltamperometric *I-U* dependencies were recorded with the EG&G/PARC potentiostat mod. 263A, controlled by IBM PC computer with the PowerStep software. In all measurements the three-electrode potentiostatic circuit was applied. The saturated (KCl) calomel reference electrode (SCE) was separated from the studied solution with a salt bridge and uncompensated ohmic drops were minimized by using the Luggin capillary. The platinum wire ($A \approx 2$ cm^2) served as a counter electrode. The serial ohmic resistance, switched between the working (streaming Hg) electrode and the appropriate slot of the potentiostat, was supported by the decade resistor RU-71 (Urania, Poland), with the maximum resolution of 0.1 Ω.

All measurements were recorded for the temperature 298.0 K, controlled by the ultrathermostat U4 (VEB MLW Prüfgeräte−Werk Medingen Dresden).

Numerical calculations were done in Turbo Pascal 7.0 with an IBM PC Pentium III machine.

3. Results of Measurements

In the following U denotes the *total* voltage applied between the working and the reference electrode while E is the *interfacial potential drop*, i.e., the total voltage corrected for the ohmic drops

$$E = U - IR_s = U - (I_f + I_c)R_s \qquad (1)$$

where R_s is the external resistance switched in series to the circuit of the working electrode and the total current I consists of the faradaic I_f and capacitive I_c contributions. Due to a negligible ohmic resistance of the studied solution (ensured by e.g., 2 mol dm^{-3} NaSCN) and of the mercury electrode one can assume that R_s is practically equal to the total ohmic resistance of the measurement circuit.

Studies were made for such a range of concentrations of NaSCN (0.7−5.0 mol dm^{-3}), for which the polarization $I-U$ curves of the Ni(II)-SCN^- electroreduction *in the absence of external serial resistance* exhibited a distinct region of a negative polarization resistance, the occurrence of which is decisive for the instabilities observed in the studied system.[19,20,23] Figure 2 shows such an exemplary $I-U$ relationship for 5 mmol dm^{-3} Ni(II) + 2 mol dm^{-3} NaSCN, a composition of a sample used in most of our experiments. One should note that the change of the total current I from the anodic (positive) to cathodic (negative) values at the foot of this dependence is caused by a contribution from the capacitive current, changing its sign when passing the potential of zero charge which for the 2 mol dm^{-3} NaSCN was estimated as close to −0.73 V.

When the appropriate serial resistance is switched into the circuit of the working electrode and one applies the linear external voltage scan toward negative values, at certain value $U_{c,2}$ a steep, substantial decrease of the cathodic current occurs, followed by its further monotonic increase with increasing

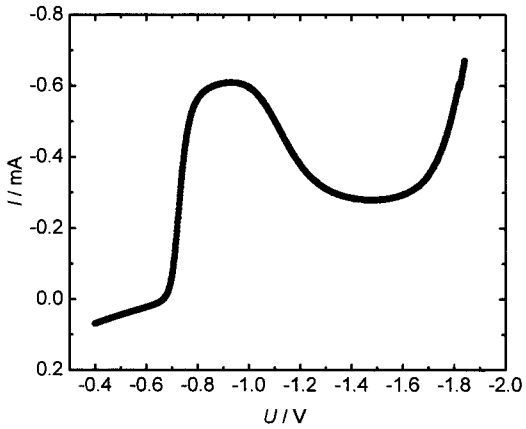

Figure 2. Exemplary $I-U$ relationship for the sample: 5.0 mmol dm^{-3} $Ni(ClO_4)_2$ + 2.0 mol dm^{-3} NaSCN, recorded at the streaming mercury electrode. Serial resistance $R_s = 0$. The region of a negative differential resistance (NDR) is observed within the potential range: ca. −1.0 and −1.5 V. Parameters of the streaming electrode: capillary flow m = 210 mg s^{-1}, internal glass capillary (= mercury electrode) diameter ϕ = 0.11 mm, length of mercury jet (directed upward) l_{max} = 2.5 mm. Temperature 298.0 K.

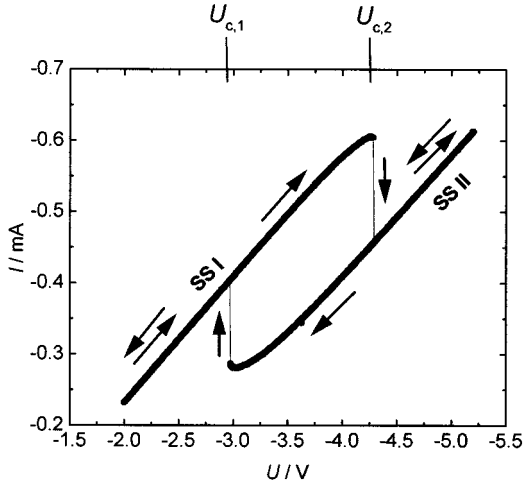

Figure 3. *Bistable* behavior in the electroreduction of the thiocyanate complexes of nickel(II) at a streaming mercury electrode, manifesting itself as the *hysteresis* in attaining the sets of "high-current" (**SS I**) or "low-current" steady-states (**SS II**) as a function of the direction of the linear voltage (U) scan. Within the interval [$U_{C,1}$ $U_{C,2}$] the system is bistable, whereas outside this region remains monostable. Composition of the studied solution and parameters of the working electrode are the same as in the caption to Figure 2, except for the serial ohmic resistance R_s = 5.5 kΩ in the electric circuit of the streaming electrode.

negative potential (see Figure 3). When the voltage scan is now reversed toward positive values, the similarly steep return to higher cathodic current is observed, but at the voltage $U_{c,1}$ more positive than $U_{c,2}$ (see again Figure 3). This *hysteresis* in the response of the system's behavior (I) vs. the smooth changes of the external control parameter (U), i.e., the manifestation of the so-called "memory effect", obviously indicates the region of *bistability* in the dynamic behavior of our system. One should emphasize that, to our knowledge, it is the first example of the bistability reported both for the Ni(II)-SCN$^-$ electroreduction and for the measurements at the streaming mercury electrode.

Changing of the resistance R_s as the experimental control parameter modifies the voltage (U) interval, within which the system exhibits bistability. Outside this region, in dependence on U and R_s, other types of the dynamic behavior can also be observed, the systematic studies of which led us to the diagram, presented in Figure 4. The borderlines show the locations of

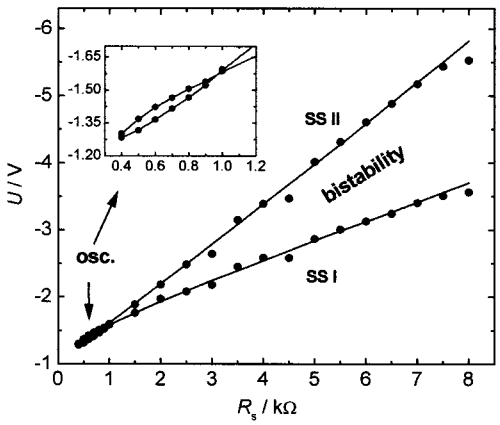

Figure 4. Stability diagram of the dynamic nonequlilibrium states observed for the electroreduction of the thiocyanate complexes of nickel(II) at a streaming mercury electrode. The lines, led through points (●) for R_s > 1 kΩ correspond to the position of the saddle-node bifurcations between the monostable and bistable behavior. **SS I** - "high current" steady-state, **SS II** - "low current" steady-state, **osc** - tiny region of oscillations. In the inset, the enlarged region of the occurrence of sustained oscillations, encircled by the curve corresponding to the Hopf bifurcation, is shown. Composition of the studied sample and parameters of the streaming electrode—the same as for Figure 2.

bifurcations, separating monostable and bistable regions involving the stable steady-states **SS I** and **SS II**. From Figure 4, it follows also that in a relatively narrow region of the control parameters the sustained oscillatory behavior was reported. Examples of two such oscillatory courses are shown in Figure 5 and one should note that their period is relatively short: ca. 42−78 ms.

Despite these various kinds of dynamic behavior observed for the Ni(II)−SCN$^-$ electroreduction, we shall focus our further analysis exclusively on the bistability, since it is definitely a new phenomenon reported for the studied process.

4. Discussion

4.1. Stable and Unstable Steady States in the Electroreduction Of Ni(II)-SCN$^-$ Complexes. The principal shape of the experimental stability diagram shown in Figure 4 is typical of numerous chemical systems which exhibit oscillations related to bistability (cf. e.g., refs 6, 24) what shows that the electrochemical process, studied by us, also belongs to this class of dynamical systems. In terms of the formalism of the nonlinear dynamics, this diagram shows two principal types of bifurcation. The tiny region of oscillations is encircled by a curve composed of the points of the Hopf bifurcation,[25] that correspond to the transition between the steady-state (stable focus) and oscillations (stable limit cycle). The lines separating the bistable and monostable behavior determine the points of a degenerated case of the *saddle-node* (SN) bifurcation,[6,25] that describes the creation, from a single stable state, of the two stable states (nodes) and one, located between, unstable steady-state (saddle). Thus, one can expect that the upper and the lower branches of the experimental diagram in Figure 3, representing the "high-current" and "low-current" *stable* dynamic steady-states of the studied process are separated by "medium-current" *unstable* steady states. Such states cannot be observed directly in the experiment, but a full diagram of states may be obtained by a simple operation performed on the original (i.e., recorded for zero ohmic resistance) $I-U$ curve from Figure 2. A translation of this curve, point by point, along the U axis, for the values of ohmic drops IR_s (with the resistance R_s = 5.5 kΩ, corresponding to experimental conditions from Figure 3) yields the folded $I-U$

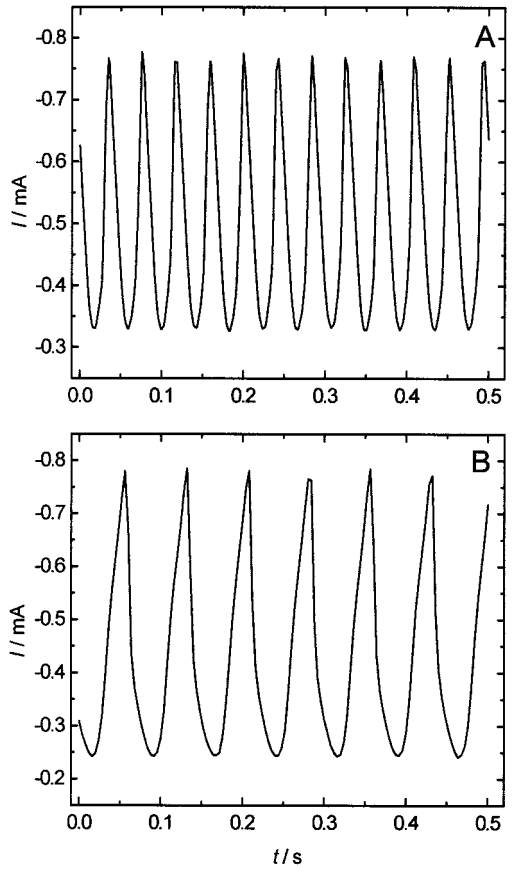

Figure 5. Exemplary sustained oscillations reported for the electroreduction of Ni(II)-SCN^- complexes at a streaming mercury electrode, for the control parameters corresponding to the region "**osc**" in Figure 4. (**A**) $U = -1.39$ V, $R_s = 0.61$ kΩ, (**B**) $U = -1.47$ V, $R_s = 0.82$ kΩ.

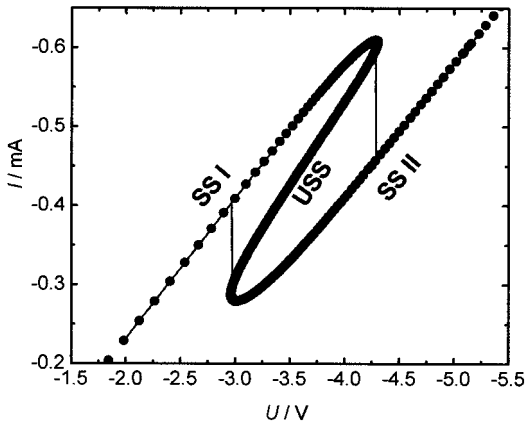

Figure 6. Full diagram of the stable (**SS I**, **SS II**) and unstable (**USS**) steady states for the electroreduction of 5.0 mmol dm^{-3} $Ni(ClO_4)_2$ + 2.0 mol dm^{-3} NaSCN at the streaming mercury electrode: (●) points obtained by the translation, on the voltage axis, of the $I-U$ curve from Figure 2, for ohmic drops IR_s (with $R_s = 5.5$ kΩ); (—) experimental curve from Figure 3.

curve, shown in Figure 6. From the comparison of this diagram with Figure 3, it follows that the branches of stable steady-states overlap perfectly for both relationships, and between them the set of *unstable* steady-states (**USS**) is now revealed. This is the full experimental characteristics of all steady-states of the Ni(II)-SCN^- electroreduction, for given conditions.

Furthermore, in view of the concordance between the characteristics of stable steady-states in Figures 3 and 6, it becomes understandable that the points of saddle-node bifurcations, visualized in Figure 4, can also be obtained from the *single* experimental $I-U$ curve from Figure 2, transformed to folded shape by translation along the U axis for the set of *assumed* resistances, i.e., without the necessity of making further measurements. We checked that the corresponding points on the stability diagram, obtained in this way, coincide very well with the bistable region in Figure 4, determined from measurements for different serial resistances.

For a more convincing and quantitative discussion of the reported phenomena and conditions underlying their occurrence we prepared numerical models of the Ni(II)-SCN^- electroreduction, which in a possibly realistic way reflect the experimental behavior of the bistable system under study.

4.2. Comparison of the Experiment and the Simulation. *4.2.1. Principal Features of the Reactant Transport to the Streaming Electrode.* The basic analytical mathematical theory of the streaming mercury electrodes was published by Koryta[26] and by Weaver and Parry.[27,28] In the simplest case of the idealized streaming electrode (cf. Figure 7A), the following assumptions are usually made: (i) the layer of the electrolyte solution in the close vicinity of the electrode, set to motion by the stream of mercury, follows exactly its surface speed, (ii) the thickness of this hydrodynamic layer of the dragged solution is greater than that of the diffusion layer; (iii) due to a short contact of the electrolyzed solution with the electrode surface the diffusion layer is so thin, that the strict cylindrical geometry of diffusion may be well approximated by a linear one: $\partial c/\partial t = D(\partial^2 c/\partial x^2)$; (iv) all concentration gradients in the solution, other than those perpendicular to the electrode surface, are negligible. On the basis of all the above assumptions one can estimate typical parameters of the mercury flow and electrolysis time, corresponding to characteristics of our experimental setup, given in the caption to Figure 2. Thus the surface velocity of mercury jet is equal to $v = m/(\pi r^2 \rho_{Hg}) \cong 1.62$ m s^{-1} (where density of mercury $\rho_{Hg} = 13.6$ g cm^{-3}). The maximum time of contact of a given portion of the solution adjacent to the moving mercury surface depends on this velocity and on the length l_{max} of the mercury jet in contact with the solution (distance **B** in Figure 1). Accordingly, the thickness of the diffusion layer increases and the associated faradaic current monotonically decreases along the length $l = [0, l_{max}]$ of the mercury jet. For its length $l_{max} = 2.5$ mm the time of contact of the solution with the electrode surface changes from zero at the glass capillary outlet to $t_{max} = l_{max}/v = 1.54$ ms at the horizontal surface of the aqueous solution. The corresponding maximum thickness of the Nernst diffusion layer $\delta_{max} = \sqrt{\pi D t_{max}}$ will then reach only 1.7×10^{-4} cm for the typical diffusion coefficient $D = 6 \times 10^{-6}$ cm^2 s^{-1}.

Now let us consider the expressions for a faradaic and the capacitive currents. For a given element of the cylindrical surface area $dA = 2\pi r dl$, located at the distance l from the capillary outlet, the *local* faradaic current is expressed by the relationship

$$dI_f(l) = nFD(dA)\left(\frac{\partial c_{ox}}{\partial x}\right)_{0,l} \qquad (2)$$

whereas the *total* faradaic current becomes an integral formula

$$I_f = 2\pi r n F D \int_0^{l_{max}} \left(\frac{\partial c_{ox}}{\partial x}\right)_{0,l} dl \qquad (3)$$

In eqs 2 and 3 the expression in brackets means the surface (at $x = 0$) horizontal gradient of the concentration of the electroactive species, measured at the vertical distance $y = l$ from the glass capillary outlet. The capacitive current which is due to a permanent charging of the new portions of flowing mercury to

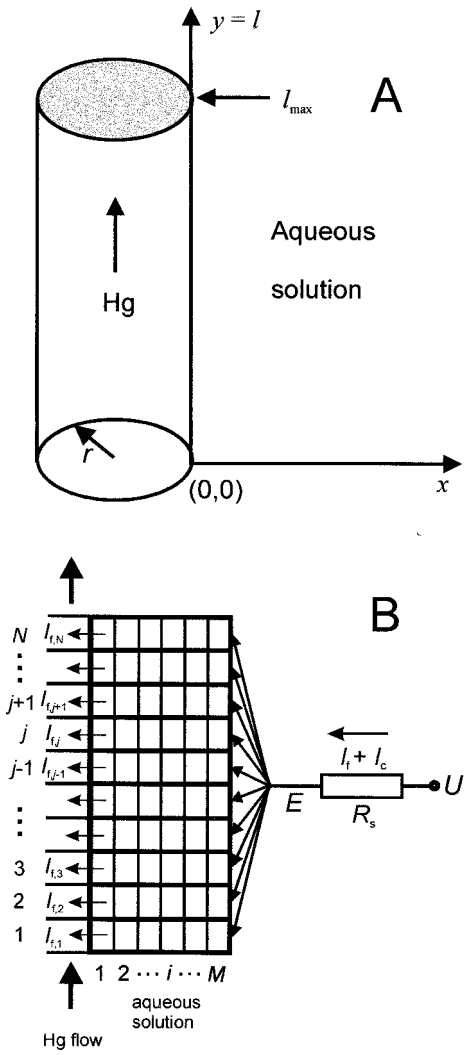

Figure 7. (**A**) Model geometry of the idealized streaming electrode. The mercury jet appears at the end of glass capillary at $y = 0$ and moves upward along the y coordinate, whereas the diffusion layer in the dragged electrolyte solution develops only along the x-coordinate; (**B**) the corresponding scheme of the space discretization for the mercury surface and the adjacent aqueous solution, where the distances along the x and y coordinates are divided into $i = 1,...,M$ and $j = 1,...,N$ spatial elements, respectively. The total faradaic current I_f consists of partial faradaic currents $I_{f,j}$ flowing through discrete segments of a surface area $\Delta A = 2\pi r\Delta l$. The permanent renewal of the electrode surface is associated with the flow of the capacitive current I_c. The potential drop $E = U - (I_f + I_c)R_s$ at the mercury/solution interface is common for all spatial elements.

an externally imposed potential is given by the relationship

$$I_C = C_d(E - E_{pzc})\frac{dA}{dt} = 2\pi rC_d(E - E_{pzc})\frac{d\,l}{d\,t} = 2\pi rC_d(E - E_{pzc})v \quad (4)$$

where A is the surface area of a cylindrical mercury jet of a radius r, C_d is the double layer capacitance (per unit area), generally dependent on the electrode potential E, and E_{pzc} is the potential of zero charge of mercury in contact with the studied solution. For exemplary data: $C_d = 25\ \mu F\ cm^{-2}$, $(E - E_{pzc}) = 1$ V and values of other parameters as assumed above one gets $I_C = 0.14$ mA. The above relationships constitute an analytical mathematical basis for the numerical (discrete) simulation model, which is described below.

4.2.2. Principles of the Numerical Model for the Process at the Streaming Hg Electrode. The model is purely numerical. Thereby, it seems noteworthy that despite numerous models elaborated for electrochemical problems (cf. e.g., refs 29−31), to our knowledge the digital simulation of the streaming electrode was not published so far.

The model electrode process was assumed in a form

$$Ox + ne \underset{k_b}{\overset{k_f}{\rightleftharpoons}} Red \quad (5)$$

where k_f and k_b are the apparent rate constants of the electroreduction and the electrooxidation steps, respectively.

The scheme of the space discretization for the surface of the mercury stream and for the adjacent solution layer, including the distribution of current and electric potential in the presence of serial ohmic resistance R_s, is sketched in Figure 7-B. According to this picture, the assumption that ohmic drops occur only in the external electric circuit and not in the solution means that all discrete segments of the electrode surface are exposed to the same potential drop at the interface, at a given time. This, in turn, implies that the variation of the faradaic current along the electrode surface in the $y = [0,...,l_{max}]$ direction is due only to the corresponding increase of the electrolysis time of the given portion of the solution, and not due to different local ohmic drops.

In the following, the total electrolysis time (i.e., measured from $t = 0$ at $y = 0$) of a given portion of the solution at the distance l will be called the *residence time* and denoted by t_{res}. In terms of the space discretization from Figure 7-B this time is given by the following relationship (if the current is calculated in the middle of every discrete $\Delta l = l_{max}/N$ segment)

$$t_{res,j} = [0.5 \times \Delta l + (j - 1)\Delta l] \times \pi\rho_{Hg}r^2/m,\ j = 1,...,N \quad (6)$$

The corresponding diffusion profile, as usual in the numerical treatment of the diffusion transport to the electrodes, was assumed to reach the maximum value of $6\delta_j$, where δ_j is the thickness of the Nernst diffusion layer for a given discrete electrode segment: $\delta_j = \sqrt{\pi D t_{res,j}}$.

Because of the ohmic drops in the external circuit the actual interfacial potential drop E is dependent on both the faradaic I_f and the capacitive I_c currents, which are also interrelated because the electrode has to be charged to this potential. The combination of the expression for the capacitive current (4) with eq 1 leads to the implicit formula

$$I_c = \frac{2\pi rC_d v(U - I_f R_s - E_{pzc})}{1 + 2\pi rC_d v R_s} \quad (7)$$

where I_f is the total faradaic current, being a sum of partial faradaic currents, flowing through discrete electrode segments

$$I_f = \sum_{j=1}^{N} I_{f,j}$$

(cf. Fig. 7B).

In turn, every this *partial* faradaic current $I_{f,j}$, as being dependent on the actual E value, is simultaneously dependent on the sum of all partial faradaic currents and the capacitive current

$$I_{f,j} = \mathbf{f}[E = U - R_s(I_c + \sum_{m=1}^{N} I_{f,m})],\quad j = 1, ..., N \quad (8)$$

where function **f** relates the faradaic current with the potential-

dependent diffusion flux of the reactant Ox

$$I_{f,j} = nF(\Delta A) f_{ox,j}(E), \quad j = 1,...,N \tag{9}$$

In terms of the finite differences notation the surface area of the electrode segment $\Delta A = 2\pi r \Delta l$ and the flux $f_{ox,j}$ is given by the relationship

$$f_{ox,j} = -\frac{k_f c_{ox,j}(1,t) - k_b c_{red,j}(1,t)}{1 + \left[\frac{k_f}{2D_{ox}} + \frac{k_b}{2D_{red}}\right]\Delta x}, \quad j = 1,...,N \tag{10}$$

In eq 10 $c_{ox,j}(1,t)$ and $c_{red,j}(1,t)$ denote the concentrations of the respective reagents in the j-th discrete spatial cell of the solution, adjacent (i.e., for $i = 1$) to the electrode surface (cf. Figure 7-B), for a model time $t = k\Delta t$ of the development of the diffusion profile, and D's denote the diffusion coefficients of respective species (Ox in the solution, Red in the mercury phase in this case). Other details of derivation of the finite differences expressions for the progress of diffusion into the bulk of the liquid phases can be found in such classical works on digital simulation in electrochemistry, as refs 29,30.

Expression 8 constitutes the set of nonlinear equations which, if ohmic resistance R_s is different from zero, can be solved iteratively with respect to the partial faradaic currents $I_{f,j}$ as the roots, with a simultaneous calculation of the capacitive current I_c, according to eq 7. Of several possible and tested by us numerical algorithms, a classical Newton's method, in the implementation published in,[32] was used as yielding the fastest and easiest convergence of iterations.

4.2.3. Model Kinetic Parameters of the Ni(II)-SCN⁻ Electroreduction. In the preliminary step of the simulations we determined the kinetic and thermodynamic characteristics of the Ni(II)-SCN⁻ electroreduction. Although we found these parameters in our previous work,[20] we recalculated them for the purposes of the present model by fitting of the $I-U$ curve, simulated according to our present model, to the experimental dependence from Figure 2. Because in this case the ohmic resistance is set to zero, and consequently $E = U$, the calculation is simplified, it involves only explicit (noniterative) calculations of the faradaic (eq 9) and the capacitive (eq 4) currents. The complex rate constants k_f and k_b of the model scheme (5) were assumed to depend on the electrode potential E in a following way

$$k_f = k_{s,1}^{app}\left\{\frac{1}{1 + \exp[P_1(E - P_2)]}\right\} \exp[-(\alpha n)_1 f(E - E_f^0)] + k_{s,2}^{app} \exp[-(\alpha n)_2 f(E - E_f^0)] \tag{11}$$

$$k_b = k_f \exp[nf(E - E_f^0)] \tag{12}$$

where $f = F/RT$, whereas P_1 and P_2 are the parameters controlling the slope and position of the region of negative resistance on the potential axis. Because the application of the streaming electrode allows to get rid of kinetic complications arising from accumulation of NiS, its inhibitory effect is here not considered and the relevant kinetic parameters used by us in ref 20 ($k_{NiS,1}$, $k_{NiS,2}$) are not included in eq 11. To obtain the best fit with most reliable parameters, for calculation of capacitive currents we used the potential-dependent differential capacitance data from our previous studies,[20] recalculated here to the potential scale of the calomel electrode. The capacitance for any desired potential E was found by the spline interpolation of these data.

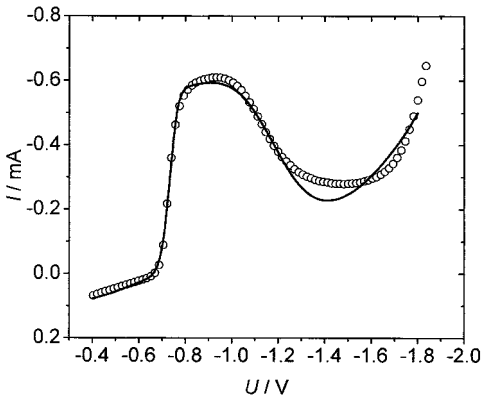

Figure 8. Comparison of the selected experimental (○) points from Figure 2 with the theoretical curve (—) simulated for the potential-dependent apparent rate constants of Ni(II)-SCN⁻ electroreduction, given by eq 11, with parameters listed in Table 1. The potential-dependent double-layer capacitance data[20] were used.

TABLE 1: Model Parameters for the Electroreduction of the 5 mM $Ni(ClO_4)_2$ + 2.0 mol dm^{-3} NaSCN at Mercury Electrodes, at 298 K (potentials referred to SCE)

model parameter	symbol	value
apparent standard rate constant of the inner-sphere Ni(II)-SCN⁻ electroreduction	$k_{s,1}^{app}$	10^{-3} cm s^{-1}
apparent standard rate constant of the outer-sphere Ni(II)-SCN⁻ electroreduction	$k_{s,2}^{app}$	4×10^{-4} cm s^{-1}
cathodic transfer coefficient associated with $k_{s,1}^{app}$	$(\alpha n)_1$	1.5
anodic transfer coefficient associated with $k_{s,1}^{app}$	$(\beta n)_1$	0.5
cathodic transfer coefficient associated with $k_{s,2}^{app}$	$(\alpha n)_2$	0.12
formal potential of the Ox/Red couple	E_f^0	−0.662 V
diffusion coefficient of Ox	D_{ox}	6.8×10^{-6} cm^2 s^{-1}
diffusion coefficient of Red	D_{red}	6.5×10^{-6} cm^2 s^{-1}
parameter 1 of the $k_f = f(E)$ dependence	P_1	−67.4 V^{-1}
parameter 2 of the $k_f = f(E)$ dependence	P_2	−0.798 V
potential of zero charge	E_{pzc}	−0.73 V

The results of this fitting are shown in Figure 8 whereas the fitted parameters of the relationship (11) are collected in Table 1. One can report some differences of selected parameters in comparison with those from ref 20. These differences may partly be due to the assumption of the ideal behavior of the streaming electrode in our present model. In reality some deviations from this imagination may occur, due to e.g., stream contraction and expansion and variable liquid velocity, as discussed by Weaver and Parry.[27] Most probably, also due to these imperfections of the behavior of the real electrode the fitted $I-U$ curve does not match perfectly the experimental dependence, but the goodness of this fit is anyway quite satisfactory for our purposes.

4.2.4. Modeling of the Hysteresis (Bistability) in the Ni(II)-SCN⁻ Electroreduction. When the nonzero serial resistance is assumed, the procedure described above was used by us for the *realistic* modeling of the course of our experiments in which bistability manifested itself *spontaneously* as a hysteresis in the $I-U$ characteristics *vs*. the direction of the linear voltage scan. The (simplified) scheme of calculations involved the following main steps:

(i) specification of the starting external voltage U

(ii) for every j-th electrode segment Δl ($j = 1,...,N$), for every k-th model time step Δt_j ($k = 1,...,N_t$), until the model times reach the values of residence times $t_{res,j}$:

(ii-a) specification of the first approximations of the faradaic currents $I_{f,j}$

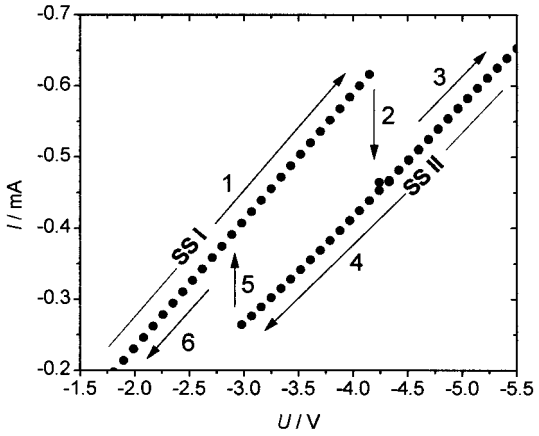

Figure 9. Hysteresis loop (bistability) in the simulated potentiodynamic behavior of the Ni(II)-SCN^- electroreduction at a streaming mercury electrode in the presence of serial ohmic resistance ($R_s = 5.5$ kΩ) in the electric circuit. The numbers at the respective arrows show the sequence in which the points, corresponding to stable steady-states, appear during the forward and the reverse voltage scan during model calculations. Characteristics of the model solution and of the streaming electrode correspond to experimental data specified in the captions to Figures 2 and 3. The potential-dependent double-layer capacitance data[20] were used for calculations of the capacitive currents.

($j = 1,...,N$)

(ii-b) calculation of $I_{f,j}$ and associated I_c, along with the progress of diffusion,

(iii) plotting of the final I_f and I_c values of currents for the given voltage;

(iv) assuming the next voltage: $U+\Delta U$ and returning to step (ii)

Concerning step (ii-a) of the above procedure it is *particularly noteworthy* that if in calculations for a given voltage U we used, as the first approximations of the partial faradaic currents, the values $I_{f,j}$ determined as solutions for the *previously* imposed voltage, we could model the desired "memory effect", i.e., the hysteresis in the system's behavior. This result is due to the characteristics of the Newton's method which exhibits convergence of iterations (if the conditions of convergence are met[33]) to this one of the existing equation's roots, which is closest to the assumed first approximation. So, if in calculations of the roots for $U = -2.50$ V we started iterations from stable steady-state currents found at the voltage equal to e.g., -2.48 V, we attained the stable steady-states from the same (upper) branch of the bistable region. This situation repeats for the next, more negative voltages, until this branch of roots stops to exist at the critical voltage $U_{c,2}$ (cf. Figure 3) and only roots from the lower current branch remain. The analogous explanation is true for the lower branch of stable steady-states, scanned from more negative voltages to the critical value $U_{c,1}$, above which only the upper branch of steady-state currents remains. This is the numerical equivalent of the "memory" which the behavior of the real system exhibits in response to smooth changes of the control parameter, when the bistable region is passed. Figure 9 shows the results of calculations, made according to principles described above. The course of this numerical experiment faithfully reproduces the dynamic behavior of the real system, shown in Figure 3. Thus, two principal conclusions can be drawn: (i) the numerical model is valid and (ii) the bistable behavior of the Ni(II)-SCN^- system at a streaming mercury electrode is indeed a result of the intrinsic instability originating from the coupling between the negative differential resistance (NDR) and the ohmic drops of the externally imposed voltage.

All the detected roots of our model equations correspond to stable steady-states (attractors) of the system, the only ones which are observable in a real experiment. In the model approach one can search also for the roots, corresponding to *unstable* steady-states, located between the upper and the lower branches of the current in Figure 9. For this purpose, the appropriate new first approximations of the faradaic currents, possibly close to intermediate roots, should be chosen and, provided the conditions of convergence are still met, these solutions could be obtained. However, for the full characteristics of the steady-states, and in order to illustrate the possibility of slightly another numerical approach, we used the modified version of our model, which is described below.

Simplified Model. The basis for the simplification was the approximation of the *total* faradaic current I_f by the product of the *partial* current $I_{f,j}$ flowing through the *middle* segment ($j = N/2$) of the streaming electrode and the total number of these segments

$$I_f \approx I_{j=N/2} \times N \tag{13}$$

Accordingly the diffusion flux f_{ox} is now calculated only for this middle segment, for the corresponding residence time of the solution, and the total faradaic current is then expressed by the following single equation

$$I_f = nFAf_{ox} \tag{14}$$

where $A = 2\pi r l_{max}$ is the *total* surface area of the cylindrical streaming electrode.

Equation 14 can be solved numerically with respect to the faradaic current as a root, and simultaneously the capacitive current is found, according to eq 7. Of all numerical methods suitable for this particular operation, the classical bisection (for optimization followed by the inverse parabolic interpolation) was found most convenient because of the following:

(i) it allowed to study systematically the subsequent (adjacent) intervals of possible faradaic currents for the existence of ***all*** roots (*both stable* and *unstable* steady-state currents) and (ii) this algorithm of searching for roots is always convergent. For further simplification of calculations the double layer capacitance was assumed constant and equal to the average value corresponding to the potential range (ΔE) of the bistable region ($\Delta E = E_2 - E_1$, where approximately $E_1 = -0.8$ V and $E_2 = -1.5$ V): $\bar{C}_d = (1/\Delta E) \times \int_{E_1}^{E_2} C_d(E)dE = 26.7\ \mu F\ cm^{-2}$.

The (simplified) scheme of calculations involved the following main steps:

(i) Dividing of the entire range of faradaic currents [0, I_{lim}] into N_F equal intervals ΔI_m ($m = 1,...,N_F$), where

$$I_{lim} = \frac{4nFD_{ox}^{1/2}m^{1/2}l_{max}^{1/2}c_{ox}^{0}}{\rho_{Hg}^{1/2}} \tag{15}$$

is the limiting faradaic current at the streaming electrode for purely diffusion-controlled conditions;[26]

(ii) specification of the starting external voltage U

(iii) for every tested m-th current interval:

(iii-a) specification of the initial first approximations of the searched faradaic current I_f as the limits of the interval [(m-1)-I_{lim}/N_F, mI_{lim}/N_F];

(iii-b) if the root of eq 14 exists within this interval:

- for every k-th model time step Δt of the residence time: calculation of I_f and associated I_c currents, along with the progress of diffusion, until the model time reaches t_{res}.
- plotting of the final I_f and I_c values for the given voltage;

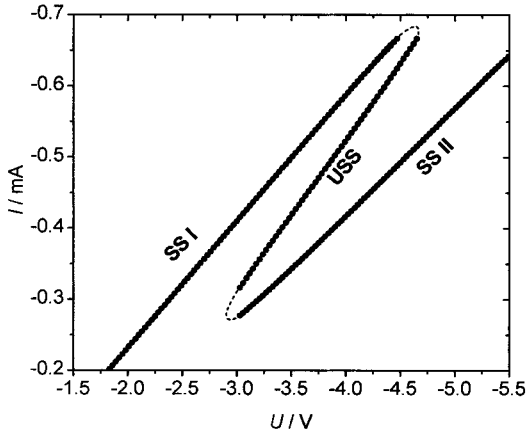

Figure 10. Theoretical diagram of the stable (upper, lower) and unstable (medium) steady-states (●) for the Ni(II)-SCN^- electroreduction, obtained from a simplified numerical model. The folded shape was approximated at the edges (- - -). Characteristics of the model solution and of the streaming electrode correspond to data specified in the caption to Figures 2, 3 and 9.

(iv) assuming the next voltage: $U + \Delta U$ and return to step (iii)

Results of the searches for the roots of eq 14, for the rate constants k_f and k_b dependent on the electrode potential as given by eq 11, and other parameters corresponding to the Ni(II)-SCN^- electroreduction from Table 1, are shown in Figure 10. The characteristic folded shape, similar to that plotted in Figure 6 for the experimental data, shows almost the full region of bistability with the inner set of unstable steady-states. Only at the edges of the fold, it is more difficult to find the roots because in these places, they are very close to each other and a very fine resolution of search is necessary. Some deviations of the course of the full modeled fold from the experimental course are obviously the result of simplification, based on eq 13, but the *principal* course of the $I-U$ shape is kept. Thus, even simplified numerical approach at least semiquantitatively reproduces the fundamental features of the dynamic nonlinear behavior of the Ni(II)-SCN^- electroreduction.

Quite satisfactory results obtained from both numerical models prove that the possible deviations from the ideal behavior of the streaming mercury electrode,[27,28] which were not considered by us, are not decisive for the occurrence of bistability in the Ni(II)-SCN^- electroreduction. Consequently, and on the basis of a quite general course of the diagram from Figure 4, one can suppose that reported sustained, regular oscillations are also the intrinsic dynamic property of the studied process. Thus, the experimental and numerical studies described in this paper constitute a satisfactory explanation of the mechanism underlying nonlinear dynamic phenomena in the Ni-(II)-SCN^- electroreduction at a streaming mercury electrode.

5. Summary

We presented new experimental realization and theoretical description of the electrochemical bistable/oscillatory system that is based on the electroreduction of thiocyanate complexes of nickel(II) at a streaming mercury electrode, in the presence of appropriate serial ohmic resistance R_s in the electric circuit. Such an electrode was applied by us for two reasons: (i) both the main and side products of the electroreduction process, which poison the electrode surface, could be quickly removed away and (ii) the system quickly attained the true single stable steady-state or sustained oscillations. To our knowledge, it is the first report on the application of the streaming mercury electrode to the study of the nonlinear dynamic behavior in electrochemical systems and the first description of bistability in the Ni(II)-SCN^- electroreduction.

We constructed the experimental bifurcation diagram in the $U-R_s$ parameter space showing the regions of monostability, bistability, and oscillations. For the quantitative proof that the observed phenomena can be explained solely by the properties of the Ni(II)-SCN^- system, the electrochemical characteristics of which exhibits the *N*-shaped region of negative differential polarization resistance (NDR), we prepared numerical procedures which allowed us both to model the hysteresis in the potentiodynamic experiments and to confirm the coexistence of the stable and unstable steady-states in the bistable region.

Acknowledgment. Financial support through Grant BW-1483/4/2000 from the University of Warsaw (Poland) is greatly acknowledged.

References and Notes

(1) Prigogine, I. *From Being to Becoming. Time and Complexity in the Physical Sciences*; Freeman: New York, 1980.
(2) Prigogine, I. *The End of Certainty. Time, Chaos and the New Laws of Nature*; The Free Press: New York, 1997.
(3) Wójtowicz, J. In *Modern Aspects of Electrochemistry*; Bockris, J. O'M., Conway, B. E., Eds.; Plenum: New York, 1973; Vol. 8, p 47.
(4) Hudson, J. L.; Tsotsis, T. T. *Chem. Eng. Sci*. **1994**, *49*, 1493.
(5) Koper, M. T. M. In *Advanced Chemical Physics*; Prigogine, I., Rice, S. A., Eds.; Wiley: New York, 1996; Vol. XCII, p 161.
(6) Krischer, K. In *Modern Aspects of Electrochemistry*, *32*; Conway, B. E., Bockris, J. O'M., White, R. E., Eds.; Kluwer/Academic/Plenum Press: New York, 1999; p 1.
(7) Schaper, H.; Köstlin, H., Schnedler, E. *J. Electrochem. Soc*. **1982**, *129*, 1289.
(8) Orlik, M.; Rosenmund, J.; Doblhofer, K.; Ertl, G. *J. Phys. Chem. B* **1998**, *102*, 1397.
(9) Orlik, M.; Doblhofer, K.; Ertl, G. *J. Phys. Chem. B* **1998**, *102*, 6367−6374.
(10) Orlik, M. *J. Phys. Chem. B* **1999**, *103*, 6629.
(11) Orlik, M. *Electrochem. Commun*. **2000**, *2*, 522.
(12) Bénard, H. *Rev. Gen. Sci. Pure Appl*. **1900**, *12*, 1261, 1309.
(13) Lord Rayleigh, *Philos. Mag*. **1916**, *32*, 529.
(14) Boissonade, J.; De Kepper, P. *J. Phys. Chem*. **1980**, *84*, 501.
(15) Krogulec, T.; Barański, A.; Galus, Z. *J. Electroanal. Chem*. **1974**, *57*, 63.
(16) Krogulec, T.; Barański, A.; Galus, Z. *J. Electroanal. Chem*. **1979**, *100*, 791.
(17) Krogulec, T.; Galus, Z. *J. Electroanal. Chem*. **1981**, *117*, 109.
(18) Krogulec, T.; Barański, A.; Galus, Z. *J. Electroanal. Chem*. **1983**, *144*, 303.
(19) Jurczakowski, R.; Orlik, M. *J. Electroanal. Chem*. **1999**, *478*, 118.
(20) Jurczakowski, R.; Orlik, M. *J. Electroanal. Chem*. **2000**, *486*, 65.
(21) *Complexometric Assay Methods with Titriplex*, 3rd. Ed.; E. Merck: Darmstadt, 1982.
(22) *Physicochemical Calendar* (in Polish), WNT: Warsaw, 1974.
(23) Koper, M. T. M.; Sluyters, J. H. *J. Electroanal. Chem*. **1993**, *352*, 51.
(24) Field, R. J.; Burger, M. (Eds.) *Oscillations and Travelling Waves in Chemical Systems*, Wiley-Interscience: New York, 1985.
(25) Strogatz, S. H. *Nonlinear Dynamics and Chaos*, Addison-Wesley: Reading, MA, 1994.
(26) Koryta, J. *Collect. Czech. Chem. Commun*. **1954**, *19*, 433.
(27) Weaver, R. J.; Parry, R. W. *J. Am. Chem. Soc*. **1954**, 76, 6258.
(28) Weaver, R. J.; Parry, R. W. *J. Am. Chem. Soc*. **1956**, *78*, 5542.
(29) Feldberg, S. W. In *Electroanalytical Chemistry*; Bard, A. J., Ed.; Marcel Dekker: New York, 1969; Vol. 3, p 199.
(30) Britz, D. *Digital Simulation in Electrochemistry*, 2nd ed.; Springer: Berlin, 1988.
(31) Speiser, B. In *Electroanalytical Chemistry*; Bard, A. J., Rubinstein, I., Eds.; Marcel Dekker: New York, 1996; Vol. 19, p 2.
(32) Marciniak, A.; Gregulec, D., Kaczmarek, J. *Numerical Procedures in Turbo Pascal for Your PC*; Nakom: Poznań 1991.
(33) Dahlquist, G.; Björck A. *Numerical Methods*, Prentice Hall: New Jersey, 1974.